

Unidirectional Mechanistic Valved Mechanisms for Ammonia Transport in GatCAB

Jiyoung Kang,[†] Shigehide Kuroyanagi,[†] Tomohiro Akisada,[‡] Yohsuke Hagiwara,[†] and Masaru Tateno^{*,‡}

[†]Graduate School of Pure and Applied Sciences, University of Tsukuba, Tennodai 1-1-1, Tsukuba Science City, Ibaraki 305-8571, Japan

[‡]Graduate School of Life Science, University of Hyogo, 3-2-1 Kouto, Kamigori-cho, Ako-gun, Hyogo 678-1297, Japan

Supporting Information

ABSTRACT: Glutamine amidotransferase CAB (GatCAB), a crucial enzyme involved in translational fidelity, catalyzes three reactions: (i) the glutaminase reaction to yield ammonia (NH_3 or NH_4^+) from glutamine, (ii) the phosphorylation of Glu-tRNA^{Gln}, and (iii) the transamidase reaction to convert the phosphorylated Glu-tRNA^{Gln} to Gln-tRNA^{Gln}. In the crystal structure of GatCAB, the two catalytic centers are far apart, and the presence of a hydrophilic channel to transport the molecules produced by the reaction (i) was proposed. We investigated the transport mechanisms of GatCAB by molecular dynamics (MD) simulations and free energy (PMF) calculations. In the MD simulations (in total $\sim 1.1 \mu\text{s}$), the entrance of the previously proposed channel is closed, as observed in the crystal structure. Instead, a novel hydrophobic channel has been identified in this study. Since the newly identified entrance opened and closed repeatedly in the MD simulations, it may act as a gate. The calculated free energy difference revealed the significant preference of the newly identified gate/channel for NH_3 transport ($\sim 10^4$ -fold). In contrast, with respect to NH_4^+ , the free energy barriers are significantly increased for both channels due to tight hydrogen-bonding with hydrophilic residues, which hinders efficient transport. The opening of the newly identified gate is modulated by Phe206, which acts as a “valve”. For the backward flow of NH_3 , our PMF calculation revealed that the opening of the gate is hindered by Ala207, which acts as a mechanistic “stopper” against the motion of the “valve” (Phe206). This is the first report to elucidate the detailed mechanisms of unidirectional mechanistic valved transport inside proteins.

1. INTRODUCTION

Translational fidelity depends on the specific attachment of amino acids to the 3'-end of their cognate tRNAs. This reaction is catalyzed by aminoacyl-tRNA synthetases (aaRSs), which are each specific for their cognate amino acid. However, most eubacteria and all known archaea lack a glutaminyl-tRNA synthetase (GlnRS), which is responsible for the formation of Gln-tRNA^{Gln} in the eukaryotic cytoplasm and in some eubacteria.^{1–4} Accordingly, such organisms without GlnRS employ an indirect pathway to synthesize Gln-tRNA^{Gln}: A nondiscriminating glutamyl-tRNA synthetase (ND-GluRS) mis-attaches Glu to the 3'-end of tRNA^{Gln}, then the mischarged Glu-tRNA^{Gln} is converted to the correctly charged Gln-tRNA^{Gln} by an enzyme, Glu-tRNA^{Gln}-dependent amidotransferase (Glu-AdT).^{1–4}

For this conversion, Glu-AdT catalyzes three reactions. The first is the hydrolysis of glutamine or asparagine to yield NH_3 or NH_4^+ (the glutaminase reaction). The second reaction is the phosphorylation of Glu-tRNA^{Gln} to yield γ -phosphoryl-Glu-tRNA^{Gln}. The third reaction is the transamidation of the activated Glu-tRNA^{Gln} into the correctly charged Gln-tRNA^{Gln}, using the ammonia species (NH_3 or NH_4^+) generated by the glutaminase reaction (the first reaction). The glutamine amidotransferase (GAT) protein family catalyzes the glutaminase reaction, and thus Glu-AdT is a member of this family.⁵ The GAT family members are further divided into three classes, on the basis of the catalytic amino acid residues responsible for the glutaminase reaction and the architecture of the glutaminase domain. Although most of the GATs belong to

the two major classes, classes I and II, Glu-AdT is categorized in the third class.⁵

Similarly, as an analogous pathway, many eubacteria employ a nondiscriminating aspartyl-tRNA synthetase (ND-AspRS) and an aspartyl-tRNA^{Asn} amidotransferase (Asp-AdT) to form Asn-tRNA^{Asn}.^{6–8} In this study, we focused on the Glu-AdT systems. Two Glu-AdTs have been found to date, i.e., the eubacterial glutamyl-tRNA(Gln) amidotransferase (Gat) CAB, consisting of the A, B, and C subunits, and the archaeal GatDE, composed of the D and E subunits.^{9,10} One subunit, GatC, is considered to be a chaperone for GatA, by helping it bind to GatB.^{1,11} The GatA and GatD subunits are responsible for producing ammonia species, while GatB and GatE catalyze two distinct reactions, i.e., the phosphorylation to activate Glu-tRNA^{Gln} and the subsequent transamidation to yield Gln-tRNA^{Gln}.^{10,12–14} The crystal structure of the complex of tRNA^{Gln}, GluRS, and GatCAB from *Thermotoga maritima* revealed that the tail body of GatB recognizes the outer corner of the L-shaped tRNA^{Gln} in a tRNA^{Gln}-specific manner.¹⁵

The crystal structures of *Staphylococcus aureus* GatCAB and *Methanothermobacter thermotrophicus* GatDE were previously determined.^{11–14} The structures revealed that the two catalytic sites for the glutaminase and transamidase reactions are approximately 30 (40) Å apart from each other in GatCAB (GatDE); thus, the ammonia species generated in the glutaminase site in GatA (D) might have to be transported

Received: June 8, 2011

Published: January 3, 2012



to the transamidase site in GatB (E). Accordingly, the presence of a molecular channel that connects the two catalytic sites for this ammonia transport has been proposed in each crystal structure (Figure 1). These channels are composed of

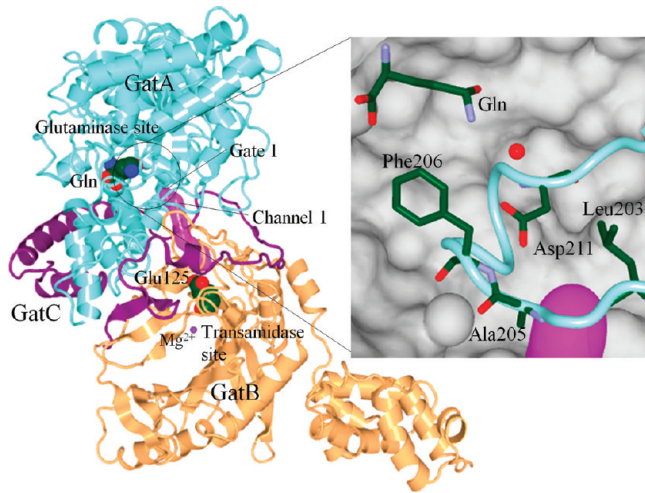


Figure 1. The left panel shows the crystal structure of *Staphylococcus aureus* GatCAB (PDB code: 2F2A). The molecular channel proposed by Nakamura et al.¹¹ is depicted by the magenta-colored tube. Its entrance is referred to as Gate 1 (see text).

hydrophilic amino acid residues. Thus, with respect to GatDE, an ammonium ion (NH_4^+), rather than an ammonia molecule (NH_3), was believed to be the species transferred through the channels.¹⁴ With regard to GatCAB, a “proton relay mechanism” was proposed for the ammonia transport, where NH_4^+ generated in the glutaminase site is deprotonated and protonated repeatedly by hydrophilic amino acid residues.¹¹ However, this hypothesis has not been experimentally examined, and thus, the detailed mechanisms for the transport have not yet been elucidated.

In this study, to investigate the mechanisms of the ammonia transport, we performed molecular dynamics (MD) simulations and free energy calculations, utilizing the crystal structure of eubacterial GatCAB, since its resolution (2.5 Å) is higher than that of the archaeal GatDE (3.2 Å) and *Thermotoga maritima* GatCAB complexed with tRNA^{Gln} and GluRS (3.35 Å). The entrance of the previously proposed channel remained closed throughout our MD simulations (in total ~1.16 μs); in fact, the calculated free energy barrier for the transport was larger. Instead, the entrance of a novel channel located adjacent to the above-mentioned (previously reported) channel opened and closed repeatedly, like a “gate”, even in 1 ns MD simulations. Therefore, we performed free energy calculations to elucidate the dependency of the protonated state of the ammonia molecule (i.e., NH_3 or NH_4^+) and whether the new entrance can actually be used for the transport. We found that the newly identified channel is preferable to the previously reported one for ammonia transport (~10⁴-fold). Since tight hydrogen bonds between NH_4^+ and hydrophilic residues of both channels would hinder effective transport, the transport of NH_3 in the newly identified channel, which is composed of hydrophobic residues, is remarkably preferable in terms of the calculated free energy barrier. Furthermore, we found that the opening of the new gate is modulated by Phe206 and that the gate acts as a “valve” to regulate the direction of ammonia transport, to achieve the asymmetric unidirectional transport. This is attributed to the

limited conformational space of Phe206 modulated by the Ala207 backbone, which functions as a mechanistic “stopper” to prevent the motion of the “valve” (Phe206).

To date, MD simulations have been performed with respect to the enzymes categorized in the two major classes of GATs (classes I and II), to investigate the mechanisms of ammonia transport.^{16–19} However, in those systems, asymmetric unidirectional transport has not been identified. Moreover, it was previously suggested that aquaporin-1 and another ammonia channel, *Escherichia coli* AmtB, may also possess “valves” for the transport of water and ammonia, respectively, although no evolutionary relationship exists between those systems and GATs.^{16,17} However, the “valve” of aquaporin-1 is not required to regulate the direction of the water flow. With respect to AmtB, the one-way transport of NH_3 was suggested, but the mechanism depends on the production of NH_3 from NH_4^+ by a Schiff base (operating the nucleophilic reaction) located in the entrance of the channel. Thus, this is the first report to describe the detailed mechanisms of a mechanistic “unidirectional valve” observed in biological macromolecular systems.

In this report, we first describe the results of the representative standard MD simulations to provide the ammonia transport mechanisms of GatCAB and then validate them by conducting multiple MD simulations (in total ~1 μs). Subsequently, we report the results of free energy calculations and thereby propose the unidirectional mechanistic valved mechanism in the ammonia transport of GatCAB.

2. COMPUTATIONAL METHODS

2.1. MD Simulations. All MD simulations were performed using AMBER 9.²⁰ The initial coordinates of the protein were obtained from the crystal structure of *S. aureus* GatCAB, which includes a glutamine bound to the glutaminase site in GatA (Protein Data Bank accession code 2F2A).¹¹ First, hydrogen atoms were added to the crystal structure, using the LEAP module implemented in AMBER 9. The ff99 force fields were then applied to the protein. The partial charges of NH_3 and NH_4^+ were calculated by a multistage restraint electrostatic potential (RESP) fit to the B3LYP/aug-cc-pvtz gas-phase calculation and yielded atomic charges for the nitrogen of NH_3 (NH_4^+) of -0.882 (-0.765) and for the hydrogen atoms of NH_3 (NH_4^+) of 0.294 (0.441), and these values were utilized in the present molecular mechanics calculations. The RESP and ab initio calculations were performed by using the RESP²¹ and Gaussian²² programs, respectively. To validate the RESP charges, the interaction energies of NH_3 (NH_4^+) and the protein side chains/backbones were obtained by employing the force field and ab initio calculations, and we confirmed that both values are consistent (see Supporting Information).

The electrostatic interactions were calculated by the particle mesh Ewald method²³ with a dielectric constant of 1.0, and a cutoff of 12 Å was used to calculate the direct space sum for the particle mesh Ewald method. The SHAKE algorithm²⁴ was used to constrain bond lengths involving hydrogen atoms. The time step for the integration was set to 1 fs. The temperature and pressure were controlled to 300 K and 1.013×10^5 Pa, respectively, using the Berendsen algorithm.²⁵ The positions of the added hydrogen atoms were optimized by the steepest descent method, and then the optimization was performed for all protein atoms.

The protein was subsequently immersed in a box of water molecules consisting of 107 910 atoms modeled by TIP3P, and

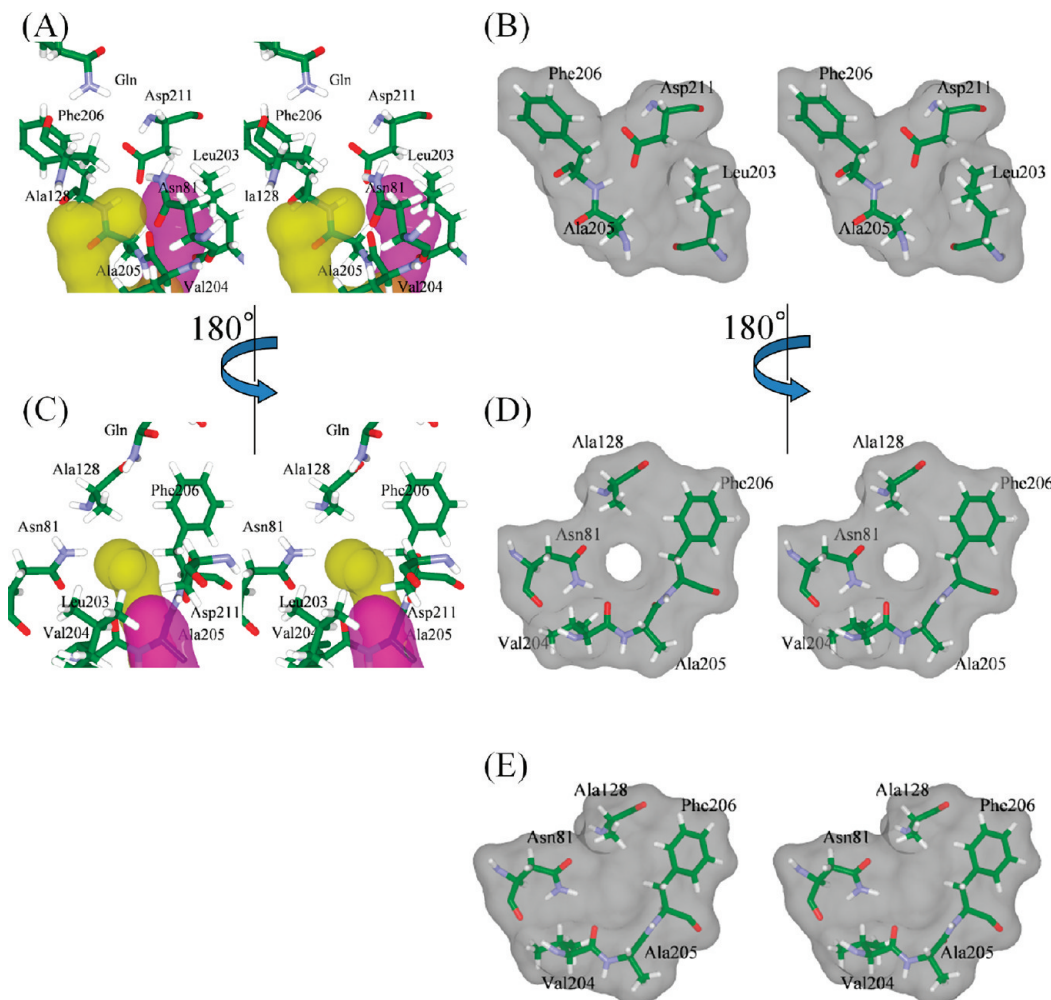


Figure 2. (A) Stereoview of the entrances of Gates 1 and 2 in the crystal structure, which is centered on Gate 1. Channels 1 and 2 are colored magenta and yellow, respectively. (B) The van der Waals surface of Gate 1 observed in the crystal structure. (C) Stereoview of the entrances of Gates 1 and 2, centered on Gate 2. This structure is a snapshot (at 100 ps) of the trajectory of SMD1 (see Supporting Information, Table S1). (D) The van der Waals surface of the open state of Gate 2 observed in SMD1 (at 100 ps). (E) The van der Waals surface of Gate 2 observed in the crystal structure.

43 Na^+ ions were added to neutralize the system (when NH_4^+ , instead of NH_3 , is involved in the system, 42 Na^+ were added). Thus, the total number of atoms of the solvated systems including NH_3 (NH_4^+) was 123 295 (123 298) atoms. To relax the configuration of the solvent water molecules, the MD simulation was performed for 10 ps at 300 K, where a harmonic constraint was applied to all protein and Na^+ atoms with a force constant of 500 kcal/mol· \AA^2 . The force constant was then reduced to 250, 125, 50, 25, 10, and 5 kcal/mol· \AA^2 in six MD simulations. The time consumed by each simulation was 2 ps. A free dynamics simulation was subsequently performed at 300 K for 1 ns. This equilibrated system was used for the potential of mean force (PMF) calculations described below.

In order to validate the results of the standard MD simulations (i.e., the twelve 1 ns trajectories corresponding to SMD1–12; see Supporting Information, Tables S2 and S3), thirty-two 3 ns MD simulations were further performed for each trajectory, starting from various snapshots in the trajectory. This scheme (i.e., the multiple MD simulations) is similar to that proposed by Auffinger et al.²⁶ (recently, Hub et al. also adopted this scheme in their analysis).²⁷ Thus, in total,

1.152 μs of additional MD simulations were performed (3 ns \times 12 \times 32 = 1152 ns).

2.2. PMF Calculations. To calculate the PMF with respect to the displacement of NH_3 (NH_4^+) along the Z-axis, which is defined to pass through two points, i.e., the initial position of the NH_3 (NH_4^+) and the active site for the transamidase reaction in GatB (the position of Mg^{2+} coordinated by Glu124 and Glu150 in GatB), the umbrella sampling technique was employed by using 40 windows in the range of 0 to 4.0 \AA . For each window, 20 ps calculations were performed. The force constants of the umbrella potential in those windows were set to 20.0 kcal/mol· \AA^2 .

Instead of a distant constraint with a harmonic potential to promote the sampling relevant to the NH_3 (NH_4^+) transport, we employed the “targeted MD” technique²⁸ implemented in AMBER9, where an additional energy term was used for the constraint, based on the root-mean-square deviation (RMSD) of a set of atoms (i.e., 5 $\text{C}\alpha$ atoms of Asn81, Ala128, Val204, Ala205, and Phe206 of GatA) in the current structure with respect to a reference structure. This technique allowed us to minimize the occurrence of nonphysical forces induced by using the distant constraint potential. When using the distant

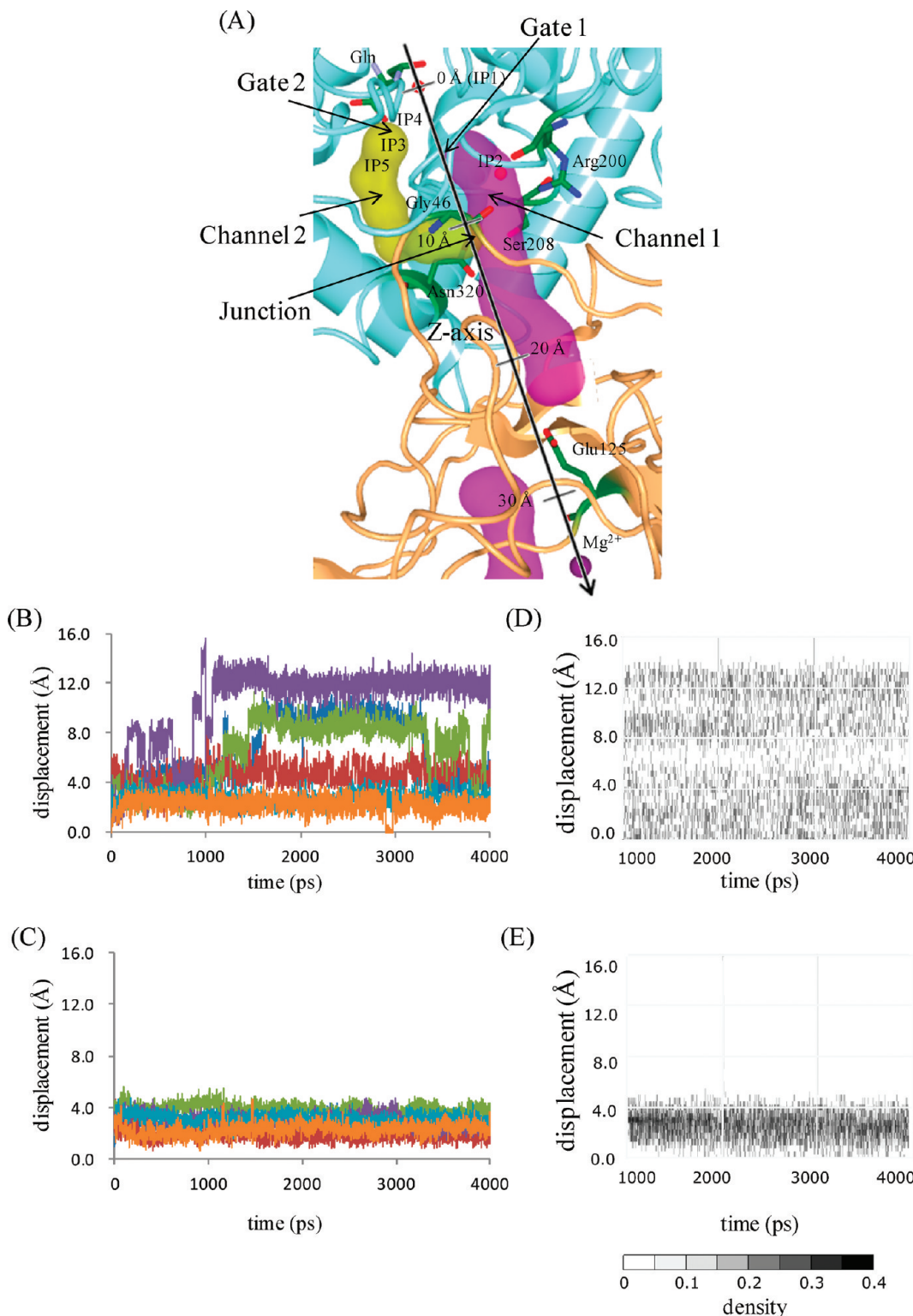


Figure 3. (A) The Z-axis connecting the initial position of the ammonia and the Mg^{2+} bound in the transamidase site. Glu125, which closes the molecular channel, is shown in a stick model. (B) The displacements of NH_3 along Z-axis obtained in the six MD simulations (SMD1–6; see Supporting Information, Table S1). The perpendicular and equatorial axes represent the displacement (\AA) and time (ps), respectively. The trajectories calculated in SMD1, SMD2, SMD3, SMD4, SMD5, and SMD6 are colored light blue, orange, dark blue, green, dark red, purple, respectively. (C) The trajectories of NH_4^+ obtained in SMD7–12, and those calculated in SMD7, SMD8, SMD9, SMD10, SMD11, and SMD12 (see Supporting Information, Table S2) are colored orange, dark red, light blue, dark blue, purple, and green respectively. (D) The distribution density map of NH_3 depicted in the above-mentioned space (i.e., time vs displacement). The snapshots were obtained from the multiple MD simulations (3 ns for each) starting from 32 initial conditions that were obtained from each trajectory of SMD1–6 (in total, $6 \times 32 \times 3000$ snapshots were used to create the density map). (E) The distribution density map of NH_4^+ . Similarly, the snapshots were obtained from the multiple MD simulations (3 ns for each) starting from 32 initial conditions that were obtained from each trajectory of SMD7–12.

constraint potential, an atom of NH_3 (NH_4^+) and another atom from the remainder of the system must be used for the constraint, and this would generate artifactitious forces on the latter atom, thereby leading to unreasonable structural changes in some cases.

The weighted histogram analysis method (WHAM)^{29,30} was used to compute the PMF. The force constant was evaluated by describing the histogram of the values of the reaction coordinates (TMD1–5; see Supporting Information, Figure S3). Thereby, we confirmed that the overlaps between the neighboring windows were sufficient, thus ensuring the convergence of PMF for each window.

2.3. Identification of Channels and Measurement of the Sizes. To find channels connecting the glutaminase and transamidase sites, we used a program, CAVER,³¹ which identifies a channel by assigning high and low penalties to grid points located close to atoms and in open space, respectively. To measure the diameter of the identified channels, we used a program, HOLE,³² in which a Monte Carlo simulated annealing is used to find a channel space where a sphere can go through. Gates were identified as being in the opened/closed states by rendering the solvent accessible surface around the gates, with respect to each MD snapshot of SMD1–12 and TMD3.

3. RESULTS AND DISCUSSION

3.1. Identification of a Novel Entrance of the Molecular Channel. In the crystal structure of *S. aureus* GatCAB (PDB code 2F2A), the glutaminase site is connected to the molecular channel, whose entrance is composed of Leu203, Ala205, Phe206, and Asp211 (Figures 1 and 2A).¹¹ A glutamine is bound to the active site, and a crystallographic water is hydrogen-bonded to N^ε of the glutamine. On the basis of the structural data, the initial position of the released ammonia was suggested to correspond to the position of the crystallographic water (the position is referred to as IP1 here; Figure 3A).¹¹ Accordingly, we replaced the above-mentioned crystallographic water with the ammonia molecule (the protonation state of the ammonia was first set to NH_3) and performed an MD simulation of GatCAB (referred to as SMD1; see Supporting Information, Table S2).

Notably, the previous biochemical experiments indicated that the enzyme exhibits glutaminase activity in the absence of tRNA, although the crystal structure does not involve the phosphorylated Glu-tRNA^{Gln}, which is to be converted to Gln-tRNA^{Gln} via a transported ammonia molecule.^{11,33,34} In the crystal structure employed for the present analysis, the Ser178 side chain forms a covalent bond with the substrate (i.e., a glutamate molecule), and all of the other important residues for the glutaminase activity are also in their proper positions to participate in the reaction, as previously reported.^{11,33} Thus, we used the above-mentioned crystal structure of GatCAB for our present analysis of the mechanisms of ammonia transport (more detailed discussions are described below).

The trajectories of the RMSDs of the C α atoms of each subunit with respect to the crystal structure, shown in Figures S4 and S5 in the Supporting Information, indicated that GatA and GatC are quite stable (the RMSD values were less than ~1.5 Å in the MD simulation). In contrast, the deviation of GatB is larger than that of the other subunits. This domain contains several long, flexible loops, which may participate in tRNA^{Gln} binding.¹⁰ Actually, the B-factors of β 12–14, α 3, and their connecting loops are over 90.¹¹ Thus, the greater fluctuation of the GatB subunit is due to its intrinsic flexibility.

With respect to the motion of the NH_3 molecule, it remained in the glutaminase site in the MD simulations and did not enter the previously reported channel (i.e., the magenta-colored channel in Figures 1 and 2) in SMD1 and SMD2 (see Supporting Information, Table S2). To quantify the motions of the NH_3 , we defined the “Z-axis”, which connects two points, i.e., the initial position of the NH_3 and the active center for the transamidase reaction in GatB (the position of Mg²⁺ bound to Glu124 and Glu150 in GatB), as shown in Figure 3A. Then, we calculated the displacement of the NH_3 along the Z-axis (Figure 3B). The displacement of 0 Å corresponds to the state where the NH_3 is located at IP1.

One reason why the NH_3 remains in the glutaminase site in the MD simulations is due to the size of the entrance of the channel, which is too small for the NH_3 molecule to enter. In fact, monitoring the van der Waals surface of the amino acid residues composing the entrance revealed that it was closed throughout the MD simulation, as seen in the crystal structure (Figure 2B). Thus, it seemed that the NH_3 molecule cannot pass through this entrance and channel; this must be further evaluated by estimating the free energy barrier for the transport (discussed later).

In contrast, we found that Asn81, Ala128, Val204, Ala205, and Phe206 of GatA can form another possible entrance, which opened and closed repeatedly in the standard MD simulations (SMD1 and SMD2) (Figure 2C and D). It should be noted here that this new putative entrance is connected to a different channel, which is attached to the previously proposed channel, as shown in Figure 3A. The junction of the two channels (i.e., the position where the two channels meet each other) is composed of interfacial residues of GatA and GatB, i.e., Ser208 and Asn320 of GatA, and Gly46 of GatB (Figure 3A).

In this report, we refer to the newly identified entrance as Gate 2, and that of the previously reported channel as Gate 1. The pathway from Gate 1 to the junction is referred to as Channel 1 (i.e., the upstream half of the previously proposed channel), and the pathway from Gate 2 to the junction as Channel 2 (i.e., the newly identified channel) (Figure 3A). Furthermore, the pathway from the junction of Channels 1 and 2 to the entrance of the transamidase site (i.e., Glu125 of GatB) is called the downstream half of the channel connecting the glutaminase and transamidase catalytic sites, which is also part of the previously reported channel, as seen in Figure 3.

3.2. Mobility of $\text{NH}_3/\text{NH}_4^+$ in Channels 1 and 2. To investigate whether these two channels can transport ammonia species, we placed an NH_3 molecule *inside* each channel. More specifically, with respect to Channel 1, the NH_3 was placed at the position occupied by the crystallographic water that hydrogen-bonds to Arg200 in GatA (this position is referred to as IP2 and is shown in Figure 3A). In terms of Channel 2, the NH_3 was placed at the position occupied by the crystallographic water that hydrogen-bonds to Asn81 in GatA (referred to as IP3, and shown in Figure 3A). These two MD simulations correspond to SMD3 and SMD5, respectively (see Supporting Information, Table S2). As a result, in SMD5, the NH_3 molecule was not transported and stayed at the initial position in the MD simulation. This lower mobility could be due to the chains of water molecules present in both channels. Actually, the channels are fully occupied by crystallographic water molecules, which form hydrogen bonds with the hydrophilic amino acid residues of the channel walls (see Supporting Information, Figure S2). In SMD3, the NH_3 molecule moved to a position specified by ~9 Å of the Z-axis

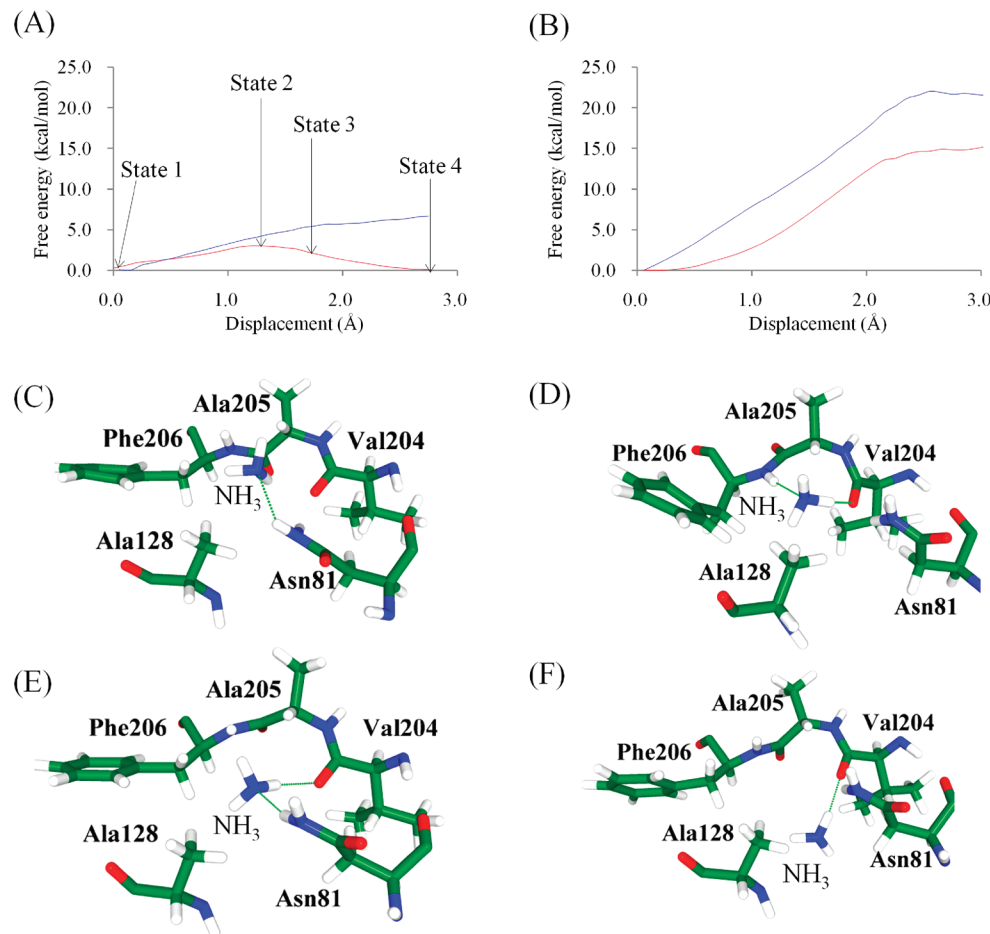


Figure 4. (A) The PMFs with respect to the displacement of NH_3 . The PMFs calculated in TMD1 and TMD3 (the NH_3 passage through Gates 1 and 2, respectively) are colored blue and red, respectively. The perpendicular and equatorial axes represent the free energy (kcal/mol) and displacement (Å), respectively. (B) The PMFs with respect to the displacement of NH_4^+ . The PMFs calculated in TMD2 and TMD4 (the NH_4^+ passage through Gates 1 and 2, respectively) are colored blue and red, respectively. (C) State 1, which is the initial structure of TMD3. The NH_3 is located in the glutaminase site (IP4). (D) State 2, which corresponds to the transition state of the NH_3 passage of Gate 2. The NH_3 forms a hydrogen bond with the amide hydrogen of Phe206. (E) State 3, where the NH_3 forms a hydrogen bond with Asn81. (F) State 4 is the final state of TMD3, where the NH_3 is transported to the inside of Channel 2.

(~1.3–3.3 ns), by pushing the water molecules in Channel 1. However, the NH_3 then returned to the initial position. Thus, since the exit from the channel is blocked by the salt bridge between Glu125 and Lys88 of GatB (Figure 3A), the water chains cannot flow in the MD simulations, due to the gate. Nakamura et al. suggested that the opening of this gate requires the binding of tRNA^{Gln} to GatB¹¹ (although the gate is not opened in the crystal structure of *T. maritima* GatCAB complexed with tRNA^{Gln} and GluRS,¹⁵ this may be because the 3'-end of tRNA^{Gln} is not bound to the transamidase site of GatCAB but the aminoacylation site of GluRS).

We removed the water molecules located in the inside of the channels and performed two further MD simulations (referred to as SMD4 and SMD6; see Supporting Information, Table S2). We first confirmed that the removal of the water molecules did not have any effect on the conformations of the three subunits (also see Supporting Information, Figure S4D and F). Then, we calculated the trajectories of the displacements of NH_3 along the Z-axis (Figure 3B). As a result, in SMD4, the NH_3 moved to a position specified by ~9 Å of the Z axis (1.3–3.3 ns) and then returned to the initial position, despite the absence of the water chain. This is why Arg200 and Asn320 of GatA were stably hydrogen-bonded with NH_3 ; therefore, the

NH_3 moved between these two amino acid residues, which prevented the transport toward the transamidase site in the MD simulation.

In contrast, in SMD6, the NH_3 entered Channel 2; interestingly, it moved up and down several times during 1 ns, and then it moved toward the transamidase site. Finally, in SMD6, the NH_3 is stabilized through a hydrogen bond with Arg323 of GatA, which is close to the channel-closing residue, Glu125, of GatB (Figure 3B). These results suggested that Channel 2 acts as the molecular channel for the ammonia transport in GatCAB.

We also examined NH_4^+ (SMD7–12; see Supporting Information, Table S2) and found that it was not appropriate for transfer, since it is trapped by the hydrophilic amino acid residues on the channel wall (Figure 3C). These results suggested that NH_3 , but not NH_4^+ , is transported; this must also be evaluated by estimating the free energy barrier for the transport (discussed below).

To validate the results of SMD1–12 by hindering the dependence on the initial structures, we further performed multiple MD simulations (in total ~1 μ s), which started from various snapshots in the 1 ns trajectory of each SMD simulation (i.e., SMD1–12) (see Supporting Information, Figures S4 and

S5) (Figures 3D and 3E). It should be noted here that GatB is an extremely flexible subunit, and thus it induces artifactitious conformational transitions of GatA and GatC in a long-time standard MD simulation. Therefore, to evaluate the effects of the large time-scale motions of the side chains in the channels, the use of multiple MD simulations starting from various initial conditions is a reasonable alternative, instead of just one long-time standard MD simulation. Thereby, one can capture the large time-scale motion of the side chains of the channels.

As a result of this analysis, we could not observe the opening motion of Gate 1 even in the $\sim 1 \mu\text{s}$ multiple MD simulations; in contrast, Gate 2 opened and closed repeatedly (gates were identified as being in the opened/closed states by rendering the solvent accessible surface around the gates, as conducted for SMD1–12; see Section 2.3). Thus, we confirmed that Gate 2 is preferred over Gate 1 for the ammonia transport. Furthermore, we created the distribution density maps of NH_3 and NH_4^+ , using all trajectories of the $\sim 1 \mu\text{s}$ multiple MD simulations (Figure 3D and E). Thereby, we also confirmed that NH_3 is more movable than NH_4^+ , which is consistent with the above-mentioned results (Figure 3B and C). More specifically, the NH_3 moved in Channel 2 and also moved toward the transamidase site, as shown in Figure 3D. These results suggested again that Channel 2 acts as the molecular channel for the ammonia transport in GatCAB.

In this manner, the results deduced from SMD1–12 were validated through the multiple MD simulations. These results are further evaluated by estimating the free energy barrier for the transport, as discussed below.

3.3. Free Energy Calculations to Evaluate Gates 1 and 2.

In the standard MD simulations discussed above, we found that the inner region of Channel 2 may be more appropriate for the ammonia transport than that of Channel 1. This propensity results from the higher hydrophobicity of Channel 2, in comparison with Channel 1. In fact, the ammonia channels identified in the crystal structures of other systems, glutamine phosphoribosylpyrophosphate (PRPP) amidotransferase,^{35,36} glucosamine-6-phosphate synthase (GlmS),³⁷ and AmtB,³⁸ are composed of hydrophobic amino acid residues. Moreover, previous theoretical studies reported that NH_3 would be easier to transport along a hydrophobic channel than NH_4^+ .^{18,39–41}

We calculated the free energy barriers for NH_3 to pass through Gates 1 and 2 by PMF calculations (see Supporting Information, Table S4). The reaction coordinate in the calculation was set to the displacement along the Z-axis mentioned above. The resultant values of the free energy barriers (ΔG) for Gates 1 and 2 were 5.6 and 2.8 kcal/mol, respectively (Figure 4A). Accordingly, the difference of the free energy barriers ($\Delta\Delta G = \Delta G_{\text{Gate}2} - \Delta G_{\text{Gate}1} = -2.8 \text{ kcal/mol}$) indicated that NH_3 is ~ 150 -fold more likely to pass through Gate 2 than Gate 1 (the Boltzmann factor was applied). This does not exclude the possibility of NH_3 passage through Gate 1. However, after passing Gate 2, the difference in the free energy for the transport increased, particularly with respect to the displacement of 3.0 Å ($\Delta\Delta G = -6.3 \text{ kcal/mol}$), where NH_3 is located inside the channels. This shows that it is more preferable for NH_3 to be transported in Channel 2 rather than Channel 1 by $\sim 8.2 \times 10^3$ -fold, which may be due to the difference in the electrostatic property of the channels, as mentioned above (i.e., the inside of Channel 1 is hydrophilic, and that of Channel 2 is hydrophobic). In other words, the most crucial reason why Gate 1 is fundamentally ruled out for ammonia transport in GatCAB is the mobility of NH_3 in the

inner regions of the channels rather than the entrance of each channel, i.e., NH_3 is trapped by hydrophilic amino acid residues in Channel 1, which prevents the transport (for the gate of each channel, the size difference is further described later).

The process of the NH_3 passage through Gate 2 is as follows. Initially, the approach of NH_3 to Gate 2 is facilitated by hydrogen-bond formation with a hydrogen atom of the δ -amine group of Asn81. The structures containing this hydrogen bond are referred to as State 1 here (Figure 4C). Then, the transition state is achieved when the displacement of NH_3 reaches 1.2 Å. In this state, the NH_3 forms a new hydrogen bond with the amide hydrogen of the Phe206 backbone, which is accomplished by the rotation of NH_3 and the conformational change of Phe206 (discussed further in Section 3.4). This structure is referred to as State 2 (Figure 4D). Subsequently, NH_3 forms a hydrogen bond with the Asn81 side chain again, although the other hydrogen atom of the δ -amine group of Asn81 participates in this case. This structure is referred to as State 3 (Figure 4E). Finally, the NH_3 passes through Gate 2 and enters Channel 2. The structure in which the NH_3 is located within the channel is referred to as State 4 (Figure 4F).

Thus, we concluded that it is easier for NH_3 to pass through Gate 2 rather than Gate 1 and that Channel 2 is more likely for the ammonia transport than Channel 1. A reason of the difference in the free energy barriers to pass through the gates is considered to result from that in the radii of Gates 1 and 2; the trajectories of the radii calculated in the free dynamics of the GatCAB (SMD1) via HOLE program³² showed that the radius of Gate 2 is larger than that of Gate 1 (Figure 5).

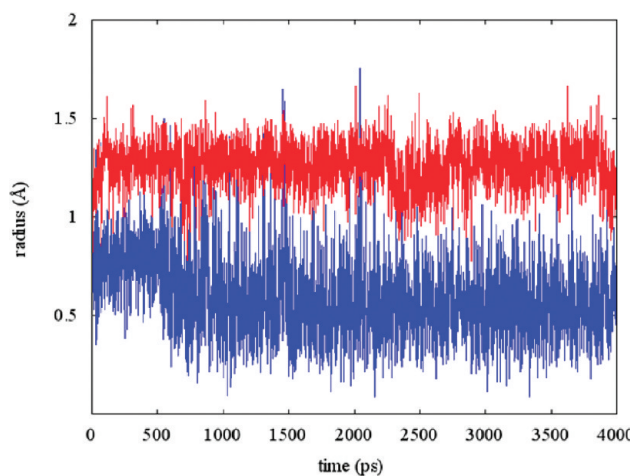


Figure 5. The trajectories of the radii of Gates 1 and 2 in SMD1 are colored blue and red, respectively. The equatorial axis represents time (ps) and the perpendicular axis shows the radii (Å), which were calculated using HOLE.³²

Moreover, we have confirmed that Gate 2 is the only one that satisfies the following requirements: (i) the gate/channel should be connected to the transamidase site, and (ii) the energy barrier for the passage of the ammonia is low enough to occur by thermal fluctuation. For (i), we used the CAVER program³¹ to automatically detect a channel connecting the two catalytic subunits. We also performed careful visual inspections of the crystal structure. As a result, no other channels that satisfy (i) and (ii) could be found.

We examined NH_4^+ in a similar way and found that the calculated free energy barriers with respect to Gates 1 and 2

were 22.0 and 14.9 kcal/mol, respectively, which are both remarkably larger than those for NH_3 (Figure 4B). This indicates that NH_3 is more preferable than NH_4^+ , which is consistent with the results obtained using SMD3–6 (Figure 3B and C). These higher free energies with respect to the NH_4^+ transport and its lower mobility within both the hydrophilic (Channel 1) and hydrophobic (Channel 2) channels, as shown in Figure 3C, suggest that NH_3 is preferable for the transport in the channel connecting the junction point and the transamidase site (actually, this region is mainly composed of hydrophilic amino acid residues). In fact, the NH_3 transport within the channel connecting the junction point and the transamidase site was observed in a standard MD simulation (SMD6) (Figure 3B).

The difference in the free energy barriers between NH_3 and NH_4^+ is supposed to arise from that in the diameter of the two molecules. In addition, the difference in the capability to form hydrogen bonds between NH_3 and NH_4^+ (i.e., the NH_3 can act as both a hydrogen-bond acceptor and donor, whereas NH_4^+ acts only as a donor) contributes to that in the free energy barriers for the transport. Although Gate 2 is broader than Gate 1, as discussed above, its diameter is still too narrow for NH_3 to enter (in fact, the NH_3 passage is not observed in SMD1 and SMD2). In State 2, which corresponds to the transition state, the hydrogen bond between NH_3 and the amide hydrogen of Phe206 promotes the passage of the NH_3 through the narrow gate (Figure 4D) by compensating for the van der Waals repulsions. In contrast, NH_4^+ cannot act as a hydrogen-bond acceptor, but just as a donor, and thereby cannot form a hydrogen bond with the Phe206 backbone (its amide hydrogen), thus increasing the free energy barrier for the transport. Due to this incapability, NH_4^+ also fails to gain sufficient stabilization to pass through the gate, since passage is facilitated by the formation of the hydrogen bond with the Asn81 side chain, as observed in State 3 of TMD3 (Figure 4E).

It should be noted here that the conformation of the Asn81 side chain in our present MD simulations differs from that in the crystal structure (Figure 4C). In the crystal structure, the N^δ of Asn81 is hydrogen-bonded with the carbonyl oxygen of its backbone, but the O^δ of Asn81 is oriented toward that of the Val204 backbone. This conformation of Asn81 could be less stable than that observed in our MD simulations. In fact, in a recent crystal structure of *S. aureus* GatCAB determined at higher resolution (1.90 Å), the conformation of the Asn81 side chain resembles that found in our MD simulations.⁴² This further suggests that our MD simulations are actually anticipatable, in terms of the functional mechanisms of GatCAB.

3.4. The Valved Mechanism for Unidirectional Transport. In the crystal structure of *S. aureus* GatCAB, the van der Waals surface of the amino acid residues composing Gate 2 showed that the entrance is closed (Figure 2E). However, the trajectory of the radii of Gate 2 in SMD1 revealed that the gate opened and closed repeatedly (Figure 5). To investigate the frequency of the opening of Gate 2, we counted the number of times that Gate 2 opened in the PMF calculation (TMD3). A dramatic difference was observed before and after the ammonia passed through Gate 2. Figure 6 shows the duration of time when Gate 2 was opened, with respect to the displacement of the ammonia along the Z-axis (here, the displacement of 0 Å corresponds to the state where the NH_3 is located in the initial position, i.e., IP1).

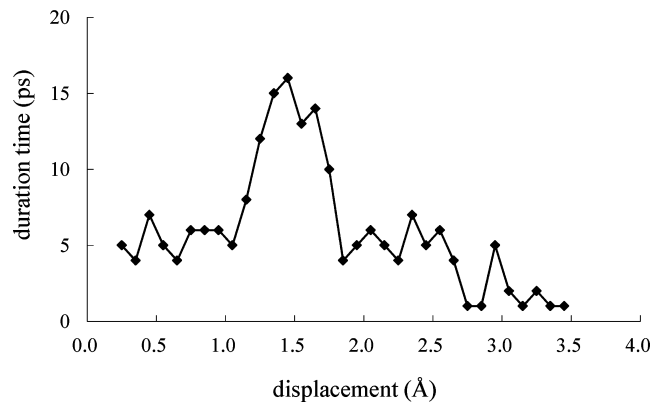


Figure 6. The duration time of the opening of Gate 2 along the displacement. The perpendicular axis represents the number of times Gate 2 opened, on the basis of the solvent accessible surface of the amino acid residues composing the gate, Asn81, Ala128, Val204, Ala205, and Phe206. The equatorial axis shows the displacement of NH_3 (Å).

This plot showed that the frequency of the opening observed before the NH_3 passing event (0.0–2.0 Å) is definitely higher than that observed after the event. This implied that the NH_3 induces conformational changes of Gate 2, to facilitate passage through it.

Furthermore, it also suggested that the NH_3 passing induces the closure of the entrance. This may prevent the “backward flow” of the NH_3 and implies a mechanism for the asymmetric transport of the ammonia.

To examine whether this mechanism can operate in asymmetric transport, we performed a further PMF calculation in which the reaction coordinates were identical to those in the above-mentioned PMF calculations, but the direction of the transport was opposite, i.e., from the inside of Channel 2 to the active site of the glutaminase reaction (TMDS). In this calculation, the conformation of Gate 2 was artificially disrupted, and these structural changes were irreversible in this PMF simulation, thus implying that the backward flow of NH_3 is prevented (the details are discussed below again). Accordingly, only the forward flow may be feasible.

The mechanism of this unidirectional transport can be explained by considering the structure corresponding to the transition state (State 2) in the PMF calculation with respect to the NH_3 passing through Gate 2 (Figure 4D). In the transition state, χ_1 of Phe206 is rotated by around 100° (from 160° to 60°) (Figure 7A), thereby expanding the gate for NH_3 to enter (Figure 8A and B). Furthermore, the rotation of χ_1 results in changes in the orientation of the amide hydrogen of Phe206, leading to the formation of the hydrogen bond between NH_3 and the amide hydrogen of Phe206, which contributes to lowering the free energy barrier (Figures 4A and 7B). After the ammonia passes through, Phe206 rotates back to the original conformation (Figure 7A). This indicates that the approach of NH_3 to Gate 2 induces conformational changes of the Phe206 side chain, which resemble a type of induced fitting. Thereby, the hydrogen bond between NH_3 and the Phe206 backbone is formed (State 2), promoting the NH_3 transport together with hydrogen-bonding with the Asn81 side chain (State 3), as discussed above (Figure 4D and E).

It should be noted here that when NH_3 moves from the glutaminase site to Channel 2, the C^β of Phe206 also moves in the same direction concertedly (Figure 8A). In contrast, in the

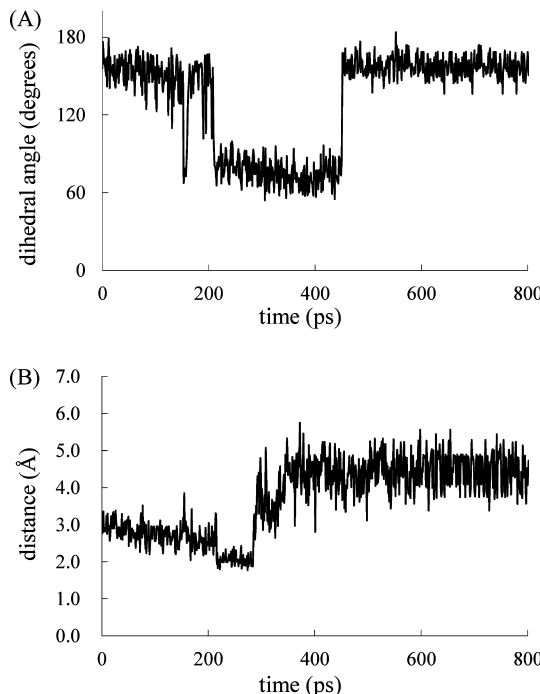


Figure 7. (A) The trajectory of χ_1 of Phe206 obtained in TMD3. The perpendicular and equatorial axes represent the dihedral angle of χ_1 ($^{\circ}$) and the simulation time (ps), respectively. (B) The trajectory of the distance between the nitrogen of NH_3 and a hydrogen attached to N^{\ddagger} of Asn81 in TMD3. The perpendicular and equatorial axes represent the distance (\AA) and the simulation time (ps), respectively.

PMF calculation to examine the backward flow of NH_3 (TMD5), this concerted motion is not observed. Instead, the original conformation of Phe206 is maintained, and thus the gate cannot be expanded. The reason why the conformation of Gate 2 was disrupted in TMD5, as mentioned above, could be due to the inappropriate reaction coordinate employed in the PMF calculation.

To investigate this issue, we performed another PMF calculation, employing the χ_1 angle of Phe206 as the reaction coordinate. As a result of the analysis, the conformation of Gate 2 was not disrupted for the backward flow of NH_3 . However, its activation barrier was estimated to be as large as ~ 100 kcal/mol, whereas that for the forward transport was consistent with the value obtained in TMD3 (see Supporting Information, Figure S6). Thus, we concluded that Gate 2 possesses the capability to transport NH_3 unidirectionally.

These results imply the unidirectionality of the C^{β} mobility: The C^{β} is allowed to move toward the inside of Channel 2 from the glutaminase site but is prohibited from moving in the opposite direction. The mechanism of this unidirectional transport can be explained by the interactions of Phe206 and the adjacent residue, Ala207. In the crystal structure, the amide hydrogen of the Ala207 backbone is located close to the C^{β} of the Phe206 side chain (the distance between the amide hydrogen and a hydrogen atom of the β -methyl group is 2.4 Å, as shown in Figure 8C). Namely, the amide hydrogen of Ala207 prevents the rotation of the χ_1 angle of Phe206 toward the direction that would lead to the steric clash with the C^{β} of Phe206 (Figure 8D).

Thus, the amide hydrogen of Ala207 acts as a mechanistic “stopper” to hinder the rotation of the χ_1 angle. The presence of the stopper causes a significant increase in the free energy

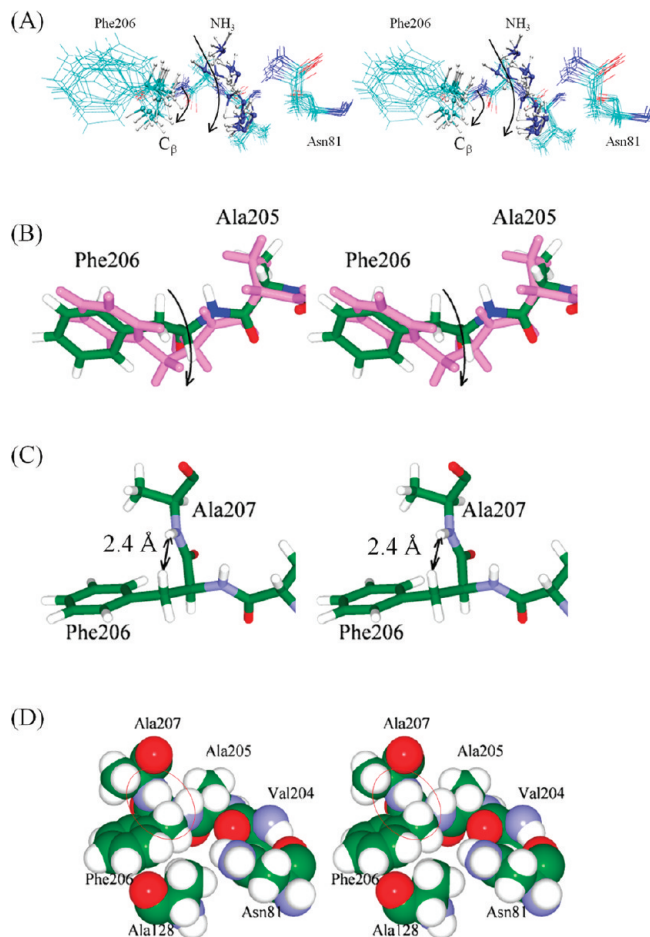


Figure 8. (A) The concerted motion of the transported NH_3 and the C^{β} of Phe206 during the NH_3 passage through Gate 2. A stereoview of the superposition of snapshots taken from TMD3 is presented. The large arrow represents the direction of the NH_3 motion, and the small arrow represents the direction of the C^{β} motion. (B) Comparison of the structure in the closed state (green) with that in the open state (magenta) (stereoview). The arrow indicates the direction of the C^{β} motion. (C) Stereoview of the conformations of Phe206 and Ala207 in the crystal structure of GatA. The Ala207 residue acts as the mechanistic “stopper” to hinder the backward rotation of the χ_1 angle of Phe206. The distance between a hydrogen atom of the β methyl group of Phe206 and the amide nitrogen of Ala207 is 2.4 Å. (D) Stereoview of the structure depicted in (C) as a CPK model. The C^{β} of Phe206 and the amide hydrogen of Ala207 are enclosed in a red circle.

barrier for the backward flow of NH_3 . Therefore, the hydrogen bond between NH_3 and the amide hydrogen of the Phe206 backbone (Figure 4D) is not formed, which also leads to the higher free energy for the backward flow.

It should be noted here that the amino acid residues responsible for the unidirectional valved mechanism (Gate 2) are strictly conserved within the GatA proteins from various species (Figure 9). However, the residues composing Gates 1 and 2 in GatA are not conserved in GatD. This suggests that the asymmetric transport mechanism presented in this study is conserved in GatA but not in GatD, i.e., another mechanism for ammonia transport could be employed in GatD.

3.5. Effects of the tRNA Binding. The previous experimental data extensively indicated that tRNA binding exerted only marginal effects on the K_m value, with respect to the glutaminase activity.^{33,34} Thus, the affinity of the substrate

GatA	<i>B. subtilis</i>	50	KARAYAKELDAALDRSEARGLLFGFPIGVKDNITVKNLRT—TCSSRLG
GatA	<i>S. aureus</i>	50	NAIKKAQELDELQKDQMDKLFGIPMGIVKDNITVNGTTRT—TCASKML
GatA	<i>D. radiodurans</i>	48	AEEAAAVGGRMGA—GETPLAGVPIVKDNITVNGTTRT—TCGSRMLA
GatA	<i>T. thermophilus</i>	45	LLEEAACD—PGPLAGLVVAVKDNITATRGLRT—TAGSRLLE
GatA	<i>A. fulgidus</i>	41	EALKMAEKYDRGEL—KGRLAGIPVAVKDNITSKGIL—TCASKMLS
GatA	<i>M. aceticivorans</i>	45	KALEQAKKIDVEGH—EGPLAGVPIAKDNISVGLPN—SCGSKILE
GatA	<i>H. marismortui</i>	11	ETTEGAD—DGPGLAGTVVAKDNITSTEGVRT—TGCSAMLE
GatA	<i>S. solfataricus</i>	48	EEVLKVEKESINK—GGKLAGVLIATKDNITSTEGIRT—TCASKML
GatA	<i>S. tokodaii</i>	48	EEVKREVREKLKNP—IATKDNITSTEGIRT—TCASKML
GatA	<i>S. acidocaldarius</i>	44	QEIDEVKNNINSK—HKGLAGVLIATKDNITSTLGI—TCASRLIE
GatA	<i>A. pernix</i>	49	EVLIDAEEAAARRWRGEARRLEGIVVVGKDNITSTFLPT—TAGSRMLD
GatA	<i>C. trachomatis</i>	48	RALLRSRIDDLLAKGDPIGILAGIPVGVKDNITHTGVKT—TCASKML
GatD	<i>M. Kandleri</i>	43	RSELGDDEHIVVKM—DNGYNVGRVDRLEKLAPEGEGH—EPSKPKME
GatD	<i>P. abyssi</i>	38	PYELSAAGDTLVKL—ENGYNI GIALEKIRRI ELEKRA—VKPVHF
GatD	<i>A. fulgidus</i>	36	—STFTNFVFLKL—DNGYNVG—FKEVLELVE—VEPFEPHL
GatD	<i>S. solfataricus</i>	40	SYS-KDRIIFVIKL—DNGYNVG I S IDN TE IKPIEKKS—SKDRESER
GatD	<i>A. pernix</i>	18	KHETSHPDTWVIKL—DNGYNI GVLYGEQDDI UVKGSLLPPTGPGLVPL
GatD	<i>N. equitans</i>	22	—EEPNTYLKL—KNGYNI GTKKSQIKEMENLINEK—KVQQ
GatA	<i>B. subtilis</i>	198	VSRYGLVFAASSLDQIGPITRNVEDNAYLQLAISGHDPMDSTSANLDVPD
GatA	<i>S. aureus</i>	198	VSRFGLVFAASSLDQIPGFLTRNVKDNIALEAISGADVNDSTAPVVDV
GatA	<i>D. radiodurans</i>	194	VSRYGLVFAASSLDQIPGFARSAAEDLALLMVIAQHDPRDTSLSLDPARF
GatA	<i>T. thermophilus</i>	185	VSRFGLIAYAASSLDQIPGMARSVRDALLMDAAGPDLPLDTSLDPPLRF
GatA	<i>A. fulgidus</i>	185	VSRYGLIAYAANSLEQIPGMADSIEDLALLLEVIAQHDTRDSTN—AGRE
GatA	<i>M. aceticivorans</i>	189	VSRYGVVAYANSLEQVPLANNVEDIAIMDVIAGYDRDSTS—IDSK
GatA	<i>H. marismortui</i>	148	VSRYGLIAYAANSLEQIPGAPVDEHADTTEOPEAAD
GatA	<i>S. solfataricus</i>	191	VSRFGLVAYAANSLEQIPGMARNAEDLGLLFSIAGPDERDATTINLNLF
GatA	<i>S. tokodaii</i>	192	VSRFGLVAYAANSLEQIPGMKAEDLALLYSIAGDPPDKDATTIHFEPOV
GatA	<i>S. acidocaldarius</i>	188	VSRYGLVAYAANSLEQIPGMKAEDLALLVLEVIAGDWDRTATTISKNE
GatA	<i>A. pernix</i>	197	VSRYGLVAYAANSLEQIPGMARSEDVMLLEVIAGDWDRTATTISKNE
GatA	<i>C. trachomatis</i>	196	VSRYGLVAFGSSLQDQGPLTTVVEDVALAMDAFAGRDIKDADTROFRGT
GatD	<i>M. Kandleri</i>	186	DT—MAFIAAALSFLVIEGLN—GPVWLVGAORSSDRPSSDAASNLIAAC
GatD	<i>P. abyssi</i>	179	DT—MGTAAALSFLMRNLG—KPVWLVGAORSSDRPSSDAAMNLICSV
GatD	<i>A. fulgidus</i>	167	DT—MHFSAAALSFLMSRSLP—KPVFWFGAORSSDRPSSDAAMNLCAA
GatD	<i>S. solfataricus</i>	179	DT—MAYTASALASFSLRSLQ—GPVWLVGSORSSDRPSSDAINLLSAV
GatD	<i>A. pernix</i>	161	DT—MAFTASALASFHKGLSPSPVLTGSQRSSDRPSSDAAFNLTSV
GatD	<i>N. equitans</i>	153	DT—MFESSAYAYALEN—IPIAFTQAORSSDRASTDAVINLFASS

Figure 9. Sequence alignment of GatA and GatD. The amino acid residues responsible for the NH₃ passage through Gate 2 (Asn81, Phe206, and Ala207) are highlighted in yellow.

for the glutaminase reaction is maintained even in the absence of tRNA, and so the conformations of the amino acid residues around the catalytic site would not be affected by tRNA binding.^{11,34} Since the amino acid residues composing the gates also reside close to the glutaminase site, the opening/closing motion of Gate 2 may be independent of the presence/absence of the tRNA. In fact, the crystal structure employed for the present analysis (PDB ID: 2F2A) represents an “active” conformation with respect to the glutaminase reaction, since a catalytic amino acid residue (Ser178) forms a covalent bond with the substrate (i.e., a glutamate molecule), which is the intermediate in the catalyst.

Moreover, the biochemical data definitely indicated that the glutaminase reaction occurs even in the absence of the tRNA: The difference in the glutaminase activity in the presence/absence of the tRNA (and ATP) is moderate (the enhancement by tRNA binding is 20–70-fold).^{33,34} Thus, the presence of the glutaminase activity without tRNA was extensively confirmed by the previous biochemical experiments. This can be understood as follows: From a biochemical point of view, the moderate enhancement of the glutaminase reaction was previously suggested to result from the occurrence of a conformational change of the protein upon the tRNA binding.^{33,34} On the basis of the crystal structure of *Staphylococcus* GatCAB, Nakamura et al. suggested that such a conformational change corresponds to that of Glu125 of GatB.¹¹ This is consistent with the discussion concerning Phe206, described earlier in this report (i.e., the conformational change of Phe206 presented in this study may occur independently upon the binding of tRNA and ATP).

Conversely, in the absence of tRNA, the closed state of Glu125 would inhibit the glutaminase reaction, since the products might be accumulated in the glutaminase reaction site. Nevertheless, the glutaminase activity is, in principle, preserved as mentioned above.^{11,33,34} This is a dilemma but must be explained. It may be why the accumulation of the products is hindered by the unidirectional valved mechanisms presented in this study, since Gate 2 can avoid the backward flow of the

products, which may also enhance the opening of Glu125 through the products dislocated into the channel connecting Gate 2 and Glu125. In this manner, Gate 2 may indirectly contribute to the enhancement of the glutaminase activity even in the absence of tRNA, thus leading to the moderate difference of the glutaminase activity.

Accordingly, the glutaminase activity could be regulated in the following two distinctive ways: (i) the opening/closing of the channel through the conformational changes of Glu125, which may be dependent on the binding of the tRNA and ATP, and (ii) the opening/closing of Gate 2, i.e., the unidirectional valved mechanism, which is fundamentally independent of the substrate binding. This functional effect of Gate 2 may compensate for the closed state of Glu125 in the absence of tRNA, as discussed earlier.

In summary, when the Glu125 gate is closed, ammonia molecules may accumulate in the channels, due to the unidirectional transport property of Gate 2. These ammonia molecules may then push the Glu125 gate, facilitating the opening motion of the gate and enhancing the glutaminase activity. Thus, the asymmetric transport mechanism of Gate 2 can provide an explanation for the moderate effects of tRNA binding on the glutaminase activity.

In the other ammonia-channeling glutamine amidotransferases,⁵ conformational changes are observed upon ammonia transport. However, GatCAB and GatDE belong to another class, which is distinct from the two major classes (classes I and II). This classification is based on the catalytic amino acid residues responsible for the glutaminase reaction and the architecture of the glutaminase domain, as mentioned earlier. Accordingly, it is very risky to predict the functional mechanisms of GatCAB and GatDE, by inference to those of the other ammonia-channeling glutamine amidotransferases, since the structural architectures are completely different between GatCAB/GatDE and the other enzymes.

3.6. Comparison of Valved Mechanisms Found in Other Systems. Valved transport mechanisms have also been proposed in other biological systems: Aquaporin-1 may also possess a valve, which acts to regulate water transport through its opening and closing motions; however, the ability to control the direction of the water flow is not required in this system.¹⁶ In another ammonia channel, *E. coli* AmtB, the presence of a valve (Ser263) located at the terminus of the channel was also proposed, to accomplish the one-way transport of NH₃; however, this mechanism depends on the production of NH₃ (appropriate for transport inside the protein) from NH₄⁺ (present in the eubacterial cytosol) by a Schiff base (Asp160) located at the entrance of the channel (i.e., the nucleophilic reaction is required for the deprotonation of the ammonia species, thereby leading to the one-way transport of NH₃).¹⁷

The valved mechanism presented in this report is also definitely different from the other conventional ones, which have been widely found in various systems.⁴³ The opening/closing motion of conventional gates is controlled by the difference in either the voltage across the cell membrane or the pH upon the binding of substrates. In contrast, the opening of Gate 2 is dynamically induced by the “direct” interactions between the ammonia molecule and the gate during the transport events, whereas the opening of the conventional gates is induced by an extrinsic stimulus, such as ligand binding, changes in pH, voltage, etc., for which the information is transferred through the protein (e.g., the conformational changes). Some of the previous/conventional types of gates

have been revealed through comparisons of static structures, such as the apo and holo states. However, the new type of gate opening found in this study should be dynamically traced with respect to the transport events.

In addition, with respect to other GAT family enzymes, such as hisH, carbamoyl-phosphate synthetase (CPS), imidazole glycerol phosphate synthase (IGPS), and glucosamine-6-phosphate synthase (GlmS), the asymmetric valved transport mechanisms presented in this study have not been found, although MD simulations were performed.^{16–19} All of these enzymes are classified into the two major classes of GATs, whereas GatCAB is categorized in a distinct class. Accordingly, the diversity of the class-specific structural architectures and the catalytic amino acid residues yields a variety of strategies for efficient ammonia transport. Thus, this is the first report to describe the detailed mechanisms of a mechanistic “unidirectional valve” observed in biological macromolecular systems.

4. CONCLUSIONS

We have found a novel gate and channel for the efficient transport of ammonia inside *S. aureus* GatCAB. The MD simulations of the protein revealed that the entrance of the newly identified channel (Channel 2) acts as a “gate” (Gate 2), which opened and closed repeatedly, even in the 1 ns MD simulations. The open/closed states of the gate are modulated by the conformational changes of the Phe206 side chain induced by interactions with an ammonia molecule. We found that the frequency of the gate opening was dependent upon the position of the ammonia. The ammonia located in the glutaminase site can promote the opening through the interaction with Phe206, whereas the ammonia within the channel cannot open the gate due to the presence of Ala207, which acts as a mechanical “stopper”; the backward flow of the ammonia induces a steric clash between the Phe206 side chain ($-C^{\beta}H_2$) and the Ala207 backbone ($-NH$). Thus, we conclude that the Gate 2 found in this study acts as the “valve” to modulate the direction of the ammonia transport. Furthermore, we have revealed that the mechanism of its opening/closing motion is novel; it could not be discovered without the dynamic traces of the transport events, whereas the conventional types of gates previously found in various biological macromolecules were detected with the use of static structures. Accordingly, this is the first report to describe the detailed mechanisms of the unidirectional mechanistic valved transport observed in biological macromolecules, which contribute to enhance the efficiency of the ammonia transport in GatCAB.

Notably, in the crystal structure of *S. aureus* GatCAB and the recently determined crystal structure of *Aquifex aeolicus* GatCAB⁴⁴ (PDB code 3H0R), Gate 2 is in the closed conformation, again indicating the critical importance of considering the dynamic properties for understanding the functional mechanisms of biological macromolecules.

■ ASSOCIATED CONTENT

Supporting Information

Tables for the setup of all MD simulations performed in the present study, the trajectories of the RMSDs of all MD simulations, evaluations of the interaction energies of ammonia and protein backbone/side chains, figures of crystal water molecules observed in the channels, and free energy profile for the backward flow. This information is available free of charge via the Internet at <http://pubs.acs.org>.

■ AUTHOR INFORMATION

Corresponding Author

*E-mail: tateno@sci.u-hyogo.ac.jp. Telephone: (+81)-791-58-0347.

Notes

The authors declare no competing financial interest.

■ ACKNOWLEDGMENTS

We thank Drs. Akiyoshi Nakamura, Isao Tanaka, and Hiori Kino for valuable scientific discussions. Computations were performed using computer facilities under the “Interdisciplinary Computational Science Program” at the Center for Computational Sciences, University of Tsukuba, the Computer Center for Agriculture, Forestry, and Fisheries Research, MAFF, Japan, and the Supercomputer Center, Institute for Solid State Physics, University of Tokyo. This work was supported by Grants-in-Aid from the Ministry of Education, Culture, Sports, Science, and Technology (MEXT) under contract no. 21340108, and from the Global Center of Excellence Program. J.K. was supported by a Research Fellowship of the Japan Society for the Promotion of Science.

■ REFERENCES

- (1) Ibba, M.; Becker, H. D.; Stathopoulos, C.; Tumbula, D. L.; Soll, D. *Trends Biochem. Sci.* **2000**, *25*, 311–316.
- (2) Ibba, M.; Soll, D. *Genes Dev.* **2004**, *18*, 731–738.
- (3) Lapointe, J.; Duplain, L.; Proulx, M. *J. Bacteriol.* **1986**, *165*, 88–93.
- (4) Wilcox, M.; Nirenberg, M. *Proc. Natl. Acad. Sci. U.S.A.* **1968**, *61*, 229–236.
- (5) Mouilleron, S.; Golinelli-Pimpaneau, B. *Curr. Opin. Struct. Biol.* **2007**, *17*, 653–664.
- (6) Akochy, P. M.; Bernard, D.; Roy, P. H.; Lapointe, J. *J. Bacteriol.* **2004**, *186*, 767–776.
- (7) Bailly, M.; Giannouli, S.; Blaise, M.; Stathopoulos, C.; Kern, D.; Becker, H. D. *Nucleic Acids Res.* **2006**, *34*, 6083–6094.
- (8) Curnow, A. W.; Ibba, M.; Soll, D. *Nature* **1996**, *382*, 589–590.
- (9) Curnow, A. W.; Hong, K.; Yuan, R.; Kim, S.; Martins, O.; Winkler, W.; Henkin, T. M.; Soll, D. *Proc. Natl. Acad. Sci. U.S.A.* **1997**, *94*, 11819–11826.
- (10) Tumbula, D. L.; Becker, H. D.; Chang, W. Z.; Soll, D. *Nature* **2000**, *407*, 106–110.
- (11) Nakamura, A.; Yao, M.; Chimnaronk, S.; Sakai, N.; Tanaka, I. *Science* **2006**, *312*, 1954–1958.
- (12) Feng, L.; Sheppard, K.; Tumbula-Hansen, D.; Soll, D. *J. Biol. Chem.* **2005**, *280*, 8150–8155.
- (13) Harpel, M. R.; Horiuchi, K. Y.; Luo, Y.; Shen, L.; Jiang, W.; Nelson, D. J.; Rogers, K. C.; Decicco, C. P.; Copeland, R. A. *Biochemistry* **2002**, *41*, 6398–6407.
- (14) Oshikane, H.; Sheppard, K.; Fukai, S.; Nakamura, Y.; Ishitani, R.; Numata, T.; Sherrer, R. L.; Feng, L.; Schmitt, E.; Panvert, M.; Blanquet, S.; Mechulam, Y.; Soll, D.; Nureki, O. *Science* **2006**, *312*, 1950–1954.
- (15) Ito, T.; Yokoyama, S. *Nature* **2010**, *467*, 612–616.
- (16) Amaro, R.; Tajkhorshid, E.; Luthey-Schulten, Z. *Proc. Natl. Acad. Sci. U.S.A.* **2003**, *100*, 7599–7604.
- (17) Amaro, R. E.; Sethi, A.; Myers, R. S.; Davisson, V. J.; Luthey-Schulten, Z. A. *Biochemistry* **2007**, *46*, 2156–2173.
- (18) Fan, Y.; Lund, L.; Yang, L.; Raushel, F. M.; Gao, Y. Q. *Biochemistry* **2008**, *47*, 2935–2944.
- (19) Floquet, N.; Mouilleron, S.; Daher, R.; Maigret, B.; Badet, B.; Badet-Denisot, M. A. *FEBS Lett.* **2007**, *581*, 2981–2987.
- (20) Case, D. A.; Cheatham, T. E.; Darden, T.; Gohlke, H.; Luo, R.; Merz, K. M.; Onufriev, A.; Simmerling, C.; Wang, B.; Woods, R. J. *J. Comput. Chem.* **2005**, *26*, 1668–1688.

- (21) Bayly, C. I.; Cieplak, P.; Cornell, W. D.; Kollman, P. A. *J. Phys. Chem.* **1993**, *97*, 10269–10280.
- (22) Frisch, M. J.; Trucks, G. W.; Schlegel, H. B.; Scuseria, G. E.; Robb, M. A.; Cheeseman, J. R.; Montgomery, J. A., Jr.; Vreven, T.; Kudin, K. N.; Burant, J. C.; Millam, J. M.; Iyengar, S. S.; Tomasi, J.; Barone, V.; Mennucci, B.; Cossi, M.; Scalmani, G.; Rega, N.; Petersson, G. A.; Nakatsuji, H.; Hada, M.; Ehara, M.; Toyota, K.; Fukuda, R.; Hasegawa, J.; Ishida, M.; Nakajima, T.; Honda, Y.; Kitao, O.; Nakai, H.; Klene, M.; Li, X.; Knox, J. E.; Hratchian, H. P.; Cross, J. B.; Bakken, V.; Adamo, C.; Jaramillo, J.; Gomperts, R.; Stratmann, R. E.; Yazyev, O.; Austin, A. J.; Cammi, R.; Pomelli, C.; Ochterski, J. W.; Ayala, P. Y.; Morokuma, K.; Voth, G. A.; Salvador, P.; Dannenberg, J. J.; Zakrzewski, V. G.; Dapprich, S.; Daniels, A. D.; Strain, M. C.; Farkas, O.; Malick, D. K.; Rabuck, A. D.; Raghavachari, K.; Foresman, J. B.; Ortiz, J. V.; Cui, Q.; Baboul, A. G.; Clifford, S.; Cioslowski, J.; Stefanov, B. B.; Liu, G.; Liashenko, A.; Piskorz, P.; Komaromi, I.; Martin, R. L.; Fox, D. J.; Keith, T.; Al-Laham, M. A.; Peng, C. Y.; Nanayakkara, A.; Challacombe, M.; Gill, P. M. W.; Johnson, B.; Chen, W.; Wong, M. W.; Gonzalez, C.; Pople, J. A. *Gaussian 03*, revision E.01; Gaussian, Inc., Pittsburgh, PA. 2003.
- (23) Darden, T.; York, D.; Pedersen, L. *J. Chem. Phys.* **1993**, *98*, 10089–10092.
- (24) Ryckaert, J. P.; Ciccotti, G.; Berendsen, H. J. C. *J. Comput. Phys.* **1977**, *23*, 327–341.
- (25) Berendsen, H. J. C.; Postma, J. P. M.; Vangunsteren, W. F.; Dinola, A.; Haak, J. R. *J. Chem. Phys.* **1984**, *81*, 3684–3690.
- (26) Auffinger, P.; Louise-May, S.; Westhof, E. *J. Am. Chem. Soc.* **1995**, *117*, 6720–6726.
- (27) Hub, J. S.; Kubitzki, M. B.; de Groot, B. L. *PLoS Comput. Biol.* **2010**, *6*, e1000774.
- (28) Schlitter, J.; Engels, M.; Kruger, P.; Jacoby, E.; Wollmer, A. *Mol. Simul.* **1993**, *10*, 291–309.
- (29) Kumar, S.; Rosenberg, J. M.; Bouzida, D.; Swendsen, R. H.; Kollman, P. A. *J. Comput. Chem.* **1995**, *16*, 1339–1350.
- (30) Kumar, S.; Rosenberg, J. M.; Bouzida, D.; Swendsen, R. H.; Kollman, P. A. *J. Comput. Chem.* **1992**, *13*, 1011–1021.
- (31) Petrek, M.; Otyepka, M.; Banas, P.; Kosinova, P.; Koca, J.; Damborsky, J. *BMC Bioinf.* **2006**, *7*, 316.
- (32) Smart, O. S.; Goodfellow, J. M.; Wallace, B. A. *Biophys. J.* **1993**, *65*, 2455–2460.
- (33) Horiuchi, K. Y.; Harpel, M. R.; Shen, L.; Luo, Y.; Rogers, K. C.; Copeland, R. A. *Biochemistry* **2001**, *40*, 6450–6457.
- (34) Sheppard, K.; Akochy, P. M.; Salazar, J. C.; Soll, D. *J. Biol. Chem.* **2007**, *282*, 11866–11873.
- (35) Krahn, J. M.; Kim, J. H.; Burns, M. R.; Parry, R. J.; Zalkin, H.; Smith, J. L. *Biochemistry* **1997**, *36*, 11061–11068.
- (36) Muchmore, C. R.; Krahn, J. M.; Kim, J. H.; Zalkin, H.; Smith, J. L. *Protein Sci.* **1998**, *7*, 39–51.
- (37) Teplyakov, A.; Obmolova, G.; Badet, B.; Badet-Denisot, M. A. *J. Mol. Biol.* **2001**, *313*, 1093–1102.
- (38) Khademi, S.; O'Connell, J. III; Remis, J.; Robles-Colmenares, Y.; Miercke, L. J.; Stroud, R. M. *Science* **2004**, *305*, 1587–1594.
- (39) Lin, Y.; Cao, Z.; Mo, Y. *J. Am. Chem. Soc.* **2006**, *128*, 10876–10884.
- (40) Luzhkov, V. B.; Almlöf, M.; Nervall, M.; Aqvist, J. *Biochemistry* **2006**, *45*, 10807–10814.
- (41) Nygaard, T. P.; Rovira, C.; Peters, G. H.; Jensen, M. O. *Biophys. J.* **2006**, *91*, 4401–4412.
- (42) Nakamura, A.; Sheppard, K.; Yamane, J.; Yao, M.; Soll, D.; Tanaka, I. *Nucleic Acids Res.* **2010**, *38*, 672–682.
- (43) Zhou, H. X.; McCammon, J. A. *Trends Biochem. Sci.* **2010**, *35*, 179–185.
- (44) Wu, J.; Bu, W.; Sheppard, K.; Kitabatake, M.; Kwon, S. T.; Soll, D.; Smith, J. L. *J. Mol. Biol.* **2009**, *391*, 703–716.